Detonation Nanodiamond and Onion-Like-Carbon-Embedded Polyaniline for Supercapacitors

By *Igor Kovalenko, David G. Bucknall,* and *Gleb Yushin**

The detonation nanodiamond is a versatile low-cost nanomaterial with tunable properties and surface chemistry. In this work, it is shown how the application of nanodiamond (ND) can greatly increase the performance of electrochemically active polymers, such as polyaniline (PANI). Symmetric supercapacitors containing PANI-ND nanocomposite electrodes with 3–28 wt% ND show dramatically improved cycle stability and higher capacitance retention at fast sweep rate than pure PANI electrodes. Contrary to other PANI-carbon nanocomposites, specific capacitance of the selected PANI electrodes with embedded ND increases after 10 000 galvanostatic cycles and reaches 640 F g^{-1}, when measured in a symmetric two-electrode configuration with 1 M H_2SO_4 electrolyte. The demonstrated specific capacitance is 3–4 times higher than that of the activated carbons and more than 15 times higher than that of ND and onion-like carbon (OLC).

1. Introduction

Nanodiamond (ND) soot is produced on a large scale by a controlled detonation of carbon-containing explosives.[1] The need to dispose of old explosives often allows ND manufacturers to acquire the ND precursors at a negative cost, which helps to keep very low production cost for the soot. Selective oxidation of sp^2 carbon in detonation ND soot by treatments with acids[1] or annealing in an oxygen-containing gaseous environment[2] allows for the fabrication of high sp^3-content ND powder. Annealing of ND powder in an inert atmosphere at temperatures above 1400 °C leads to their graphitization and formation of onion-like carbon (OLC).[1,3] Applications of ND powder have shown rapid growth during the last few years.[1,4] In particular, applications of ND-polymer or ND-metal composite coatings with enhanced strength, impact resistance, scratch resistance, thermal stability and conductivity, have been explored.[4a,4j–l,4o,4q,4r] OLC–polymer composites have been used efficiently for electromagnetic shielding as well as fluorescence-induced indicators of high energy protons.[1,4j,4l] The OLC as a polymer filler offers attenuation of electromagnetic radiation similar to that of multi-walled carbon nanotubes (MWCNT), but is much easier to disperse in a variety of solvents. ND bound with a chemotherapeutic agent and embedded within a porous polymer films may allow for a modulated release of therapeutics within areas of diseased tissue.[4b,4c,4h,4p]

Due to their high surface area, good mechanical properties, low cost and relatively high conductivity of as-produced ND soot and OLC, they offer attractive properties for energy storage applications, such as electrochemical capacitors, also known as supercapacitors. These energy storage devices complement batteries for applications where higher power or longer cycle-life is desirable, such as hybrid transportation systems or power grid applications.[5] In contrast to hundreds of publications devoted to CNT-based capacitors, there are only a few papers that have reported electrochemical studies of ND and OLC.[6] The specific capacitance of ND and OLC is in the range of 20–40 F g^{-1},[6] which is similar to that of multi-walled CNTs,[6a,7] but lower than that of microporous carbons (80–250 F g^{-1})[8] and significantly lower than that of conductive polymers (200–1500 F g^{-1}).[5a,9] Polyaniline (PANI) is one of the most common electrochemically active conductive polymers that has one of the highest capacitance reported.[9e,9g] Two of the common disadvantages of conductive polymers (such as PANI) are the relatively slow charge and discharge time compared with porous carbons and, more importantly, the lack of long-term stability, presumably due to the significant volume changes during the capacitor operation and the resultant decrease of electrode electrical conductivity. In order to overcome such shortcomings, the use of CNT-PANI,[9a,9b] porous carbon-PANI[9e,9g,10] and graphene-PANI[11] composites have been studied by several research groups in the past few years and significant improvements in both the stability and the PANI capacity have been observed. In all these studies PANI was chemically or electrochemically deposited on the conductive carbon surface. Yet, most of the studies were not systematic and no clear understanding of the mechanisms of performance enhancement or the optimum structure of the PANI-carbon composites were reported. Furthermore, despite many attractive attributes of detonation ND, there are no reports on ND or OLC-polymer composite materials for supercapacitor applications.

The objective of this work was to demonstrate the feasibility of manufacturing ND-PANI (or OLC-PANI) composite with attractive electrochemical properties and reveal the effects of the carbon content and its distribution on the PANI performance. Moreover, by changing the electrical conductivity of the

[*] I. Kovalenko, Dr. D. G. Bucknall, Dr. G. Yushin
School of Materials Science and Engineering
Georgia Institute of Technology
Atlanta, Georgia 30332 (USA)
E-mail: yushin@gatech.edu

DOI: 10.1002/adfm.201000906

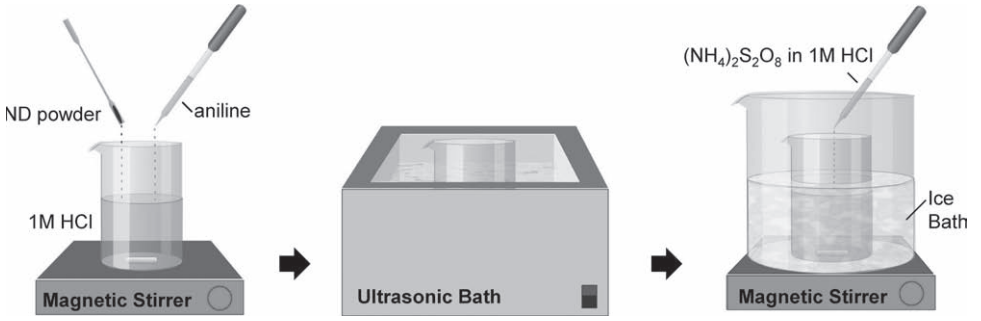

Figure 1. Schematic of the PANI and PANI-ND composites' synthesis process.

nanocarbon (purified sp^3 ND vs. sp^2 OLC) we aimed to reveal the importance of the electrical conductivity, morphology and the surface structure of the additives for the composite electrochemical cycling stability.

2. Results and Discussion

The synthesis protocol employed included several stages and is schematically shown in **Figure 1**. Initially, aniline was added dropwise into 1 M HCl, which was continuously stirred at 200 rpm. For the formation of composites, ND powder was slowly added at the same time. The ND suspension produced was sonicated in an ultrasonic bath for 30 min and then placed in an ice bath. Ice-cold ammonium persulfate solution was then added drop wise into the continuously stirred and chilled aniline-ND suspension over 1.5 h, leading to the synthesis of PANI or PANI-ND composites.

Figure 2a shows a representative image of a typical ND powder sample, with particles ranging from 4 to 20 nm and an average size of around 5 nm. We used three types of the powder: as-produced ND soot (Figure 2b), purified ND (Figure 2c) and annealed ND, which we also call OLC (Figure 2d). Electrically conductive ND soot is black in color and contains sp^3 ND core particles, coated either with sp^2 amorphous or graphitic shells (Figure 2b). Selective oxidation of the sp^2 carbon leads to pristine and electrically resistive light grey ND particles[2] without any graphitic carbon visible in high resolution transmission electron microscopy (TEM) studies (Figure 2c). High-temperature annealing of either the ND soot or the purified ND particles leads to the formation of branched nanocarbon powders with highly ordered graphitic walls and no residual sp^3 carbons (Figure 2d).

Scanning electron microscopy (SEM) studies showed the formation of either spherical or elongated PANI nanoparticles with dimensions of 100–500 nm (**Figure 3**). The shape and size of the PANI-ND (or PANI-OLC) composite particles were very similar to that of pure PANI, irrespective of the amount of carbon additives. The surface of the pure PANI particles was rather smooth (Figure 3a). Interestingly, the incorporation of the nanoparticles led to some visible roughness on the PANI surface (Figure 3b, c).

The incorporation of ND particles into the PANI structure had a significant impact on both the electrode performance and stability, when tested in supercapacitors. **Figure 4** shows

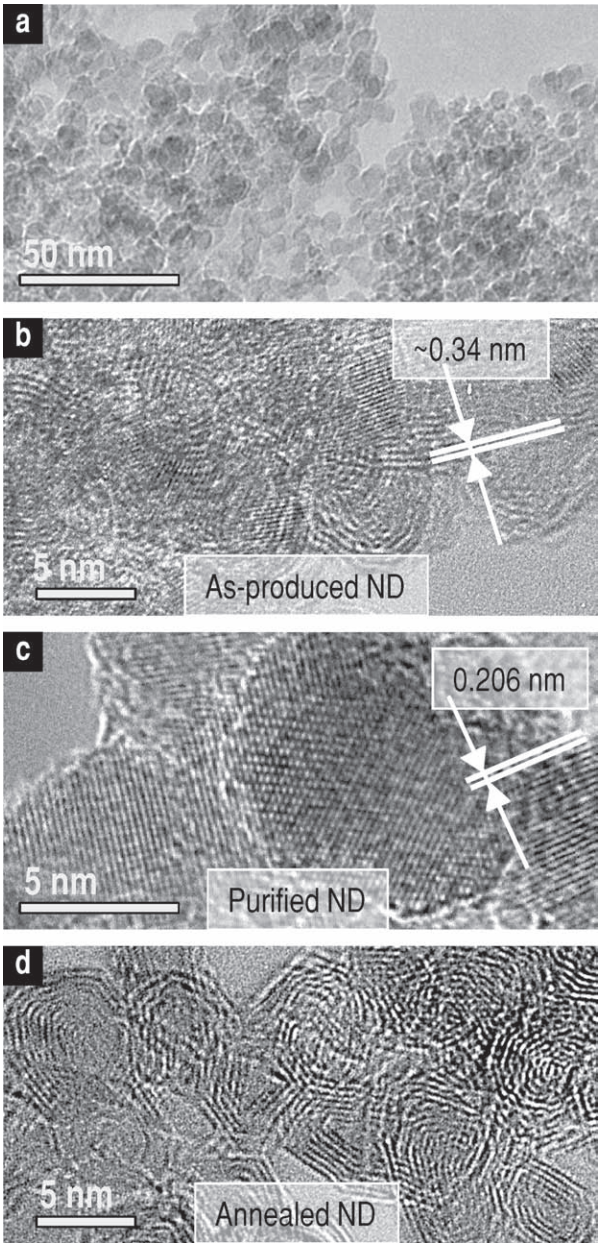

Figure 2. TEM images of the ND samples: a) low-resolution micrograph of ND powder, b) ND soot, c) purified ND, d) annealed ND (OLC)

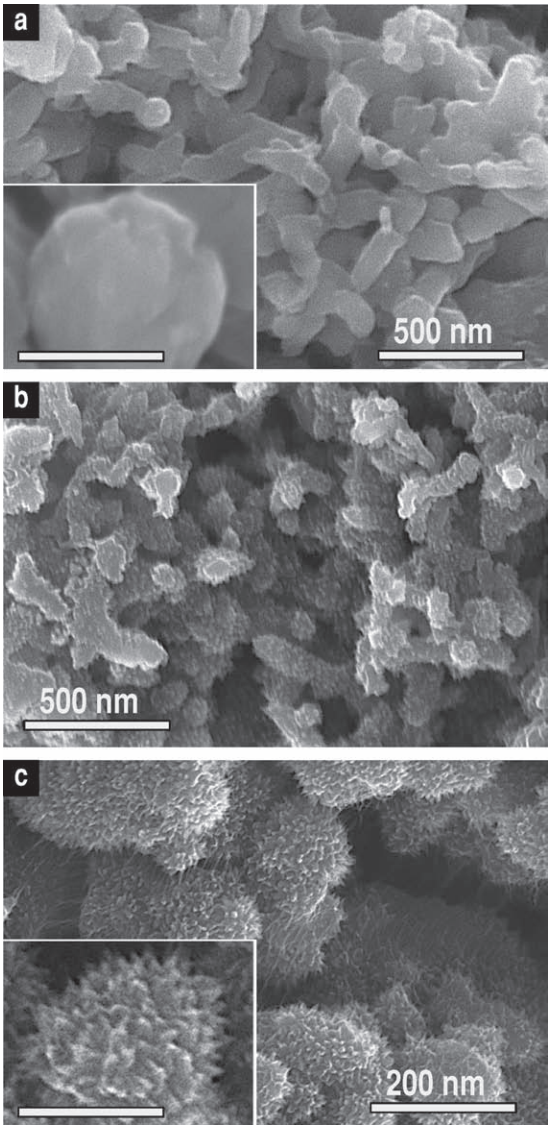

Figure 3. SEM images of the synthesized a) PANI and b,c) PANI-ND composite samples. The scale bar in the insets in (a) and (c) is 100 nm.

the results of the cyclic voltammetry (CV) measurements performed on the PANI and PANI-ND electrodes in a symmetrical two-electrode configuration.

PANI specific capacitance is known to depend on the preparation conditions, thickness and the morphology of a carbon-PANI composite. It also strongly depends on the measurement technique (measurements in a symmetric two-electrode cell configuration vs. individual electrode measurements in a three-electrode cell configuration). The difference by the factor of 3-to-4 between such measurements is common. For example, CNT-PANI composite (20 wt% CNT) shows specific capacitances of ~250 F g^{-1} in symmetric two-electrode cells[9a] and up to ~1100 F g^{-1} in thee-electrode cells.[9b] The values for the initial PANI capacitance (obtained using three-electrode measurements within –0.2 to +0.7 V or 0 to +0.7 V potential windows vs. Hg/Hg_2SO_4) were reported to reach 820 F g^{-1} for PANI nanowire network grown on stainless steel[9f] and 1220 F g^{-1} for PANI whiskers grown on mesoporous carbon.[9g] A recent paper reported initial capacitance of PANI of up to 2200 F g^{-1} for ultra-thin layers of PANI deposited on mesoporous carbon.[9e] It should be noted that the authors deposited very small amount of PANI on carbon (1.5 wt%) and assumed the invariance of porous carbon weight and capacitance (8 F g^{-1}) after PANI electrodeposition,[9e] which may or may not be a correct assumption. Unfortunately, the electrodeposition might be prohibitively expensive for many supercapacitor applications. Many recent reports on a low-cost chemical synthesis of PANI have also shown rather low values of the PANI capacitance of ~240 F g^{-1},[11a] ~200 F g^{-1},[9c] and ~115 F g^{-1},[11d] presumably due to errors in the pure PANI preparation.

In our experiments, pure PANI electrodes initially exhibited an average capacitance of 470 F g^{-1} in symmetrical cells. This capacitance is one of the highest values ever reported for a two electrode cell configuration,[9b] and indicates very good synthesis conditions employed (Figure 1). As observed by others, pure PANI electrodes showed significant degradation after 10,000 galvanostatic cycles (Figure 4a). The long-term cycling affected both the integrated-average capacitance value and the shape of the CV curve. The PANI initially exhibited a quasi-rectangular voltammogram in the –0.6 to 0.6 V voltage range with small peaks at ~ ±0.4 V. In contrast, after cycling only a single large peak at ~0 V appears with negligibly small capacitance observed at ±0.6 V (Figure 4a). The slight asymmetry of the curve is related to the galvanostatic cycling being performed between 0 and 0.6 V. In this case one electrode was repeatedly exposed to higher voltages, which may lead to a stronger degradation.

All the PANI-ND (or PANI-OLC) composite electrodes with embedded nanoparticles exhibited significantly better capacitance retention after multiple cycles than pure PANI electrodes (Figure 4b–f). **Figure 5** summarizes the capacitance values before and after 10 000 cycles. In addition to the pure PANI electrode and PANI electrodes with imbedded ND particles, this figure also shows the performance of PANI electrodes containing mechanically mixed annealed ND powder (3 wt%). These electrodes exhibited the same performance as the pure PANI electrodes. The embedding of any of the ND samples in the amount of 3–28 wt% into the PANI structure resulted in a similar or even higher integrated-average specific capacitance values after cycling. This is quite a remarkable achievement, which demonstrates significant potential for applications of ND additives in supercapacitors. By comparison, other carbon-polymer composites show significant degradation of capacitance, with CNT-PANI composite (20 wt% CNT) showing 10% degradation after 3000 cycles,[9a] CNT-PANI composite (27 wt% CNT) showing 6% degradation after 1500 cycles,[9d] activated carbon coated with a thin PANI layer showing 10% degradation after 1000 cycles (both cycled within a voltage range from 0 to 0.6 V),[10] mesoporous carbon-PANI composite showing 7% degradation after 3000 cycles,[9g] 50 nm PANI nanoparticles deposited on porous carbon monolith showing 12% degradation and dense PANI film deposited on nonporous carbon showing as high as 75% degradation after 1200 cycles.[9e]

Contrary to our initial expectations, the purified and non-conductive ND performed better than highly conductive OLC (Figure 5) and allowed for the increased composite stability,

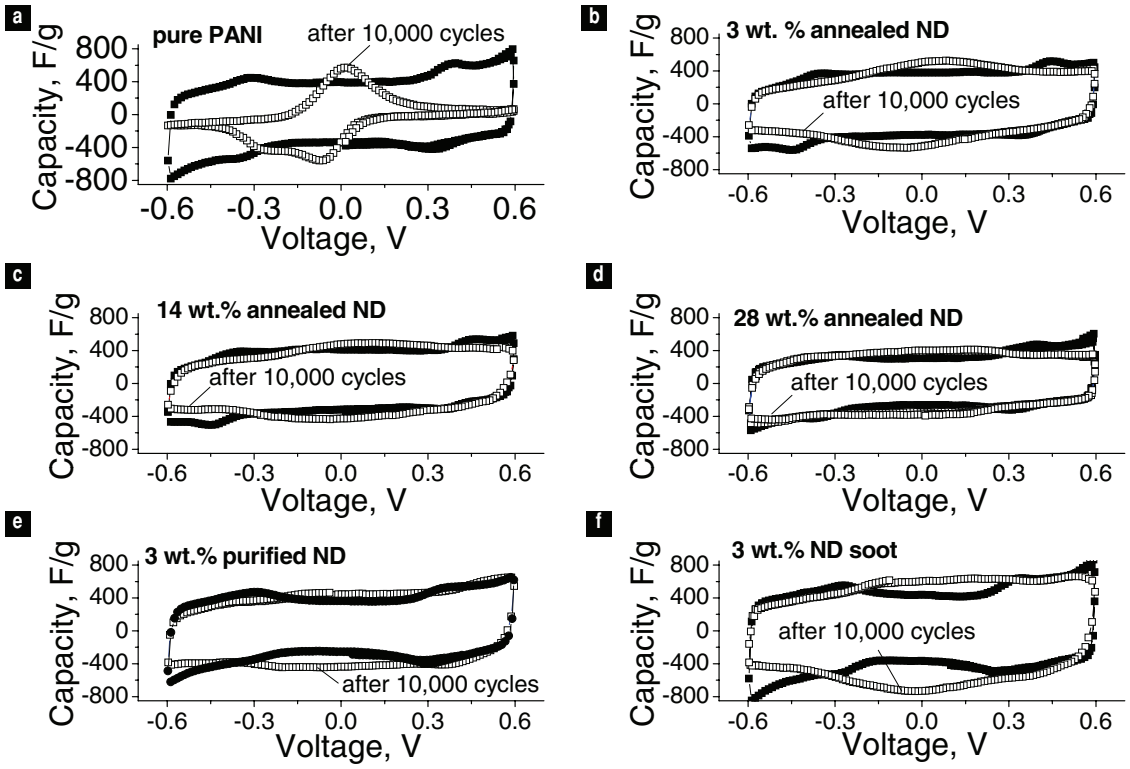

Figure 4. CV of the PANI-based electrodes recorded at the sweep rate of 1 mV s^{-1} in a symmetric two-electrode configuration before and after 10,000 cycles: a) pure PANI, b) PANI with embedded 3 wt% OLC, c) PANI with embedded 14 wt% OLC, d) PANI with embedded 28 wt% OLC, e) PANI with embedded 3 wt% purified ND, f) PANI with embedded 3 wt% ND soot.

as evidenced by the rectangular shape of the CV after cycling (compare Figure 4b and 4e). The Faradeic reactions occurring during charging and discharging of the supercapacitor, are known to cause swelling and contraction of PANI, which may lead to the continuous electrode disintegration, the loss of the electrical contact between the electrode particles and the eventual capacity loss with cycling.[9a,9d,9e,9g,10] Higher voltages lead to larger volume changes and consequently stresses in the electrodes, and therefore degradation of capacitance with increasing cycling is much more pronounced at higher potentials, as clearly seen in Figure 4a. The incompressible nanopowder additives embedded into soft PANI likely serve as a toughening agent thereby minimizing the volume changes within the PANI particles. Thus, the strength of bonding between the additives and PANI may influence the long-term electrode stability.

Unlike a highly graphitized surface of OLC containing a small concentration of defects achieved by a heat-treatment at 1800 °C,[6a,12] the purified ND surface has a very high concentration of oxygen-containing surface functionalities.[2] The interaction between the OLC and aniline monomers is likely to be dominated by the π stacking interactions between the benzene rings of the aniline molecules and the graphitic OLC surface. Due to the small OLC size and thus high surface curvature, the number of anchor points between the polymerized aniline and OLC is not expected to be high,[13] leading to the relatively weak bonding between the PANI and OLC additives. By contrast, much stronger interactions are expected to exist between the purified/oxidized ND and the polymerized aniline due to the hydrogen bonding between the amino groups in aniline and the carboxylic group of the ND surface. We, therefore, hypothesize that these stronger interactions are responsible for the improved stability of the composite electrodes with purified ND additives.

The low specific capacitance of OLC[6a] is expected to decrease the PANI-OLC composite capacitance for higher OLC content. The experimentally observed dependence (Figure 5), however, does not follow a simple linear combination rule. In fact, increasing the embedded OLC content from 3 to 14 wt%, slightly increased the composite capacitance. A similar phenomenon was also observed by others and is believed to be related to a higher concentration of the accessible electrochemically active sites in thinner PANI films deposited onto the conductive carbon surface.[11a,11d,11f] Another interesting observation is a very high specific capacitance observed in PANI-ND soot composite electrode (Figure 4f, 5). Compared with two-electrode measurements performed on PANI-CNT and PANI-graphene electrodes (230–250 F g^{-1} initial capacity),[9a,11a] PANI-ND soot electrodes demonstrated specific capacitance 2.5–3 time higher (640 F g^{-1} after 10 000 cycles, Figure 5). The ND soot has very low tap density of 0.1 g cc^{-1} (compare with 0.5 g cc^{-1} for purified ND and 0.1 g cc^{-1} for OLC/annealed ND). In contrast to oxidized ND, which commonly consists of isolated/weakly bound particles[2,4d] which can be efficiently compacted, particles in ND soot are often bridged with sp^2 carbon[2] which increases the separation distance between the

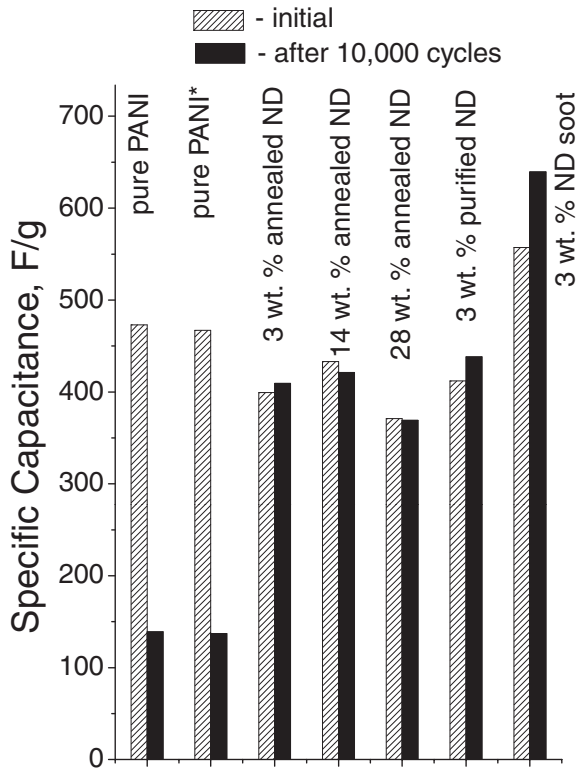

Figure 5. Integrated average specific capacitance of the synthesized samples before and after 10 000 cycles. Pure PANI* sample contains 3 wt% annealed ND mechanically mixed with PANI particles. Other samples contain ND embedded into the PANI particles. The specific capacitance was calculated from the cyclic voltammetry curves recorded at the sweep rate of 1 mV s^{-1} in a symmetric two-electrode configuration.

particles, thus preventing high density packing, and more importantly contributes to the formation of the electrically connected carbon matrix within PANI. In contrast to OLC, which has hydrophobic surface and is difficult to disperse in aqueous solutions, ND soot has a much more polar/hydrophilic surface and forms significantly more stable suspensions in HCl. This behavior is known to be crucial for the formation of a well-dispersed distribution of ND particles in polymers[4d] and may explain higher electrochemical utilization of PANI in this sample.

In order to get additional insights into the effects of the surface chemistry of the additives on the performance of the composites, we have performed extensive impedance spectroscopy studies. The impedance spectra of electrochemical capacitors (that have very high electrical conductivity of the electrodes) can be simulated by the transmission line equivalent circuit, as originally proposed by de Levie.[14] In this case the simulated Nyquist plot of impedance will contain two segments—the 45° segment and the nearly vertical line at low frequency.[14] The distortions from this idealized behavior are commonly modeled via a constant phase element.[15] In addition, poor current collector–electrode interface can be modeled as an R-C loop[16] in series with a transmission line circuit. An equivalent series resistance (ESR) is an important characteristics of the cell measured at high frequency where the imaginary component of the complex impedance becomes zero. As expected, pure PANI electrodes (**Figure 6a**) exhibited significantly lower equivalent series resistance (ESR) after 10 000 cycles and a high frequency semi-circuit loop, characteristic of a poorer electrode and electrode-current collector interface.[16] All the composite samples showed either unchanged (Figure 6c,d) or even decreased (Figure 6e, f) ESR after cycling. The ESR decrease was most evidently observed

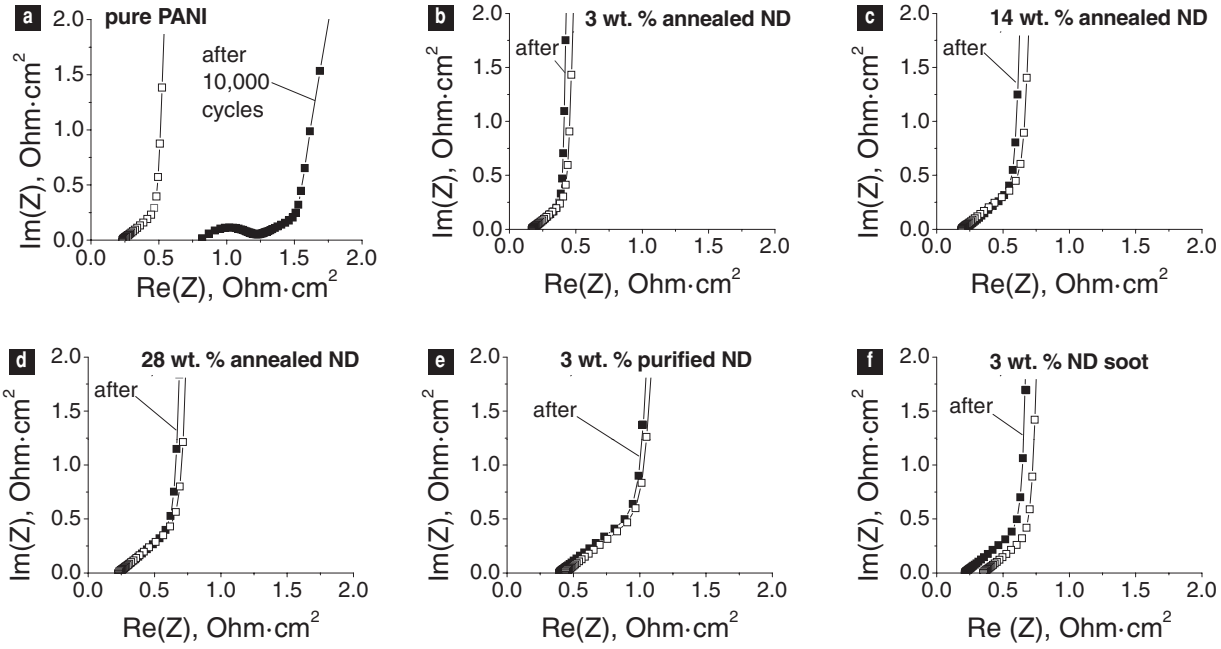

Figure 6. Nyquist plots of the PANI-based electrodes: a) pure PANI, b) PANI with imbedded 3 wt% OLC, c) PANI with imbedded 14 wt% OLC, d) PANI with embedded 28 wt% OLC, e) PANI with embedded 3 wt% purified ND, f) PANI with embedded 3 wt% ND soot.

in the PANI-ND soot composite electrodes (Figure 6f) and correlates with the corresponding increase in the specific capacitance (Figure 5). The highest ESR before cycling was observed in the PANI-purified ND sample. The highest ESR indicates the lowest electrical conductivity of this sample, as expected for non-conductive ND additives. Interestingly, the ESR and thus the electrical conductivity of the electrodes do not noticeably change with higher OLC content (compare Figure 6b–d). The conductive OLC particles are clearly fully coated with PANI and their percolation is prevented by the surface polymerization process utilized.

The 45° segment in the Nyquist plot (Figure 6) is related to the diffusion of the ions into the bulk of the electrode particles.[16] The increased length of this segment indicates a higher resistance faced by the ions during their transport into the particle core. When OLC, purified ND and ND soot composite samples with the same additive content are compared (Figure 6b, e, f), the PANI-purified ND sample demonstrates the highest electrolyte resistance, followed by the PANI-ND soot sample, with the OLC possessing the lowest resistance. Higher electrolyte resistance qualitatively correlates with the expected strength of the interaction between PANI chains and the additive particles.

Since higher concentrations of conductive additives (OLC) coated by PANI evidently does not increase the electrode electrical conductivity or decrease the electrolyte ionic resistance within the electrode pores (Figure 6b–d), such additions will not positively affect the supercapacitor ability to quickly charge or discharge. During in situ composite synthesis, PANI coats the OLC particles, which precludes their percolation needed for the improved electrical conductivity of the electrode. The SEM observations also revealed that the electrode preparation process (which included pressure-rolling, also called calendaring) caused the distortion and compression of PANI and PANI-ND (PANI-OLC) particles in the electrode, partially sealing the large pores between the particles. In contrast, the addition of conductive OLC via mechanical mixing may allow both improved electrical conductivity of the electrode and improved ion transport (the latter is due to the pores remaining between the incompressible OLC particles added into the electrode mix). Indeed, CV curves recorded at different rates (1–100 mV s^{-1}) indicate similar decrease in capacitance and similar distortion of the curves for pure PANI and PANI-OLC electrodes with as high as 28 wt% in situ embedded OLC (compare **Figure 7a** and b). By contrast, when we prepared a new electrode of PANI-purified ND (3 wt%) composite mechanically mixed with 24 wt% OLC, it demonstrated significantly better charge-discharge characteristics. Furthermore, after 10,000 charge-discharge cycles the shape of the CV curves recorded at different rates practically did not change–they remain highly symmetrical with the small pseudocapacitance peaks at ~ ±0.4 V visible (Figure 7c). Clearly, mechanical mixing of the PANI composite with highly conductive nanocarbon additives leads to the greatly improved power characteristics.

Thus, there is a synergy in the combination of the two approaches of the ND addition: embedding ND into the PANI matrix for increasing the specific capacitance and cycle life and mechanical mixing ND with the PANI for increasing the charging/discharging time constant and further improvements in the cycle stability. Moreover, the tunable properties of the ND utilized allow for optimum performance in accomplishing each of the

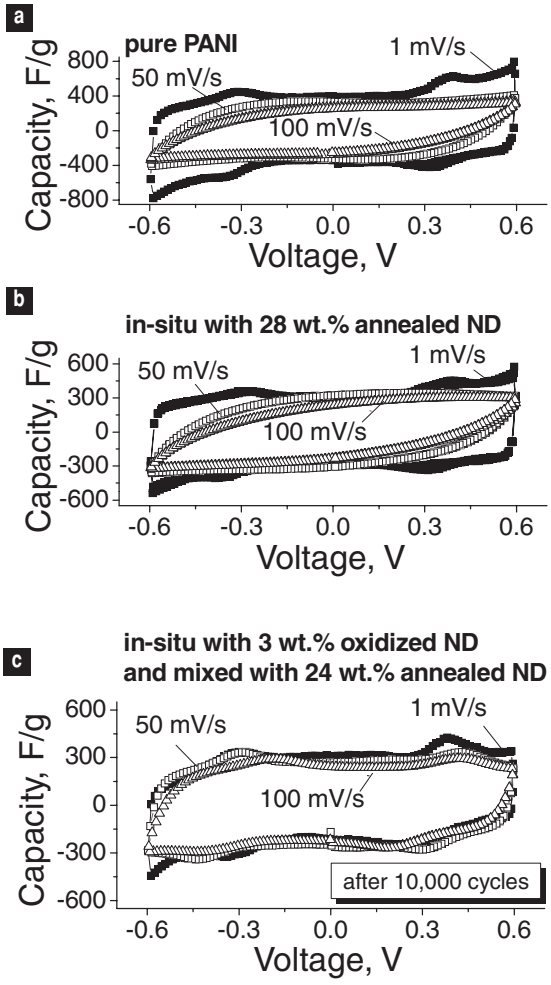

Figure 7. CV of the selected PANI-based electrodes recorded at different sweep rates in a symmetric two-electrode configuration: a) pure PANI before long-term cycling, b) PANI with embedded 28 wt% OLC before long-term cycling, c) PANI with embedded 3 wt% purified ND and mixed with 24 wt% OLC after 10 000 cycles.

independent tasks: high temperature annealing in the inert environment for the electrode conductivity improvements and the formation of carboxylic moieties on the ND surface for better dispersion within the PANI matrix, and stronger ND-PANI interactions.

In order to investigate changes in the PANI after cycling that led to the observed performance degradation (Figure 4a) we performed two tasks. First, we disassembled the degraded cell, cleaned the electrode with the DI water and ethanol, re-mixed and re-rolled it to create new electrodes and re-tested in symmetric cells (**Figure 8**). Secondly, we performed Fourier transform infrared spectroscopy (FTIR) studies on PANI before and after the cycling (**Figure 9**). The results of both measurements suggest that simple mechanical electrode degradation is mostly responsible for the capacitance fading (Figure 4a). The shape of the CV curve of the electrode degraded after 10,000 cycles completely restores once the electrical contact within the electrode is re-established (Figure 8). In fact, the cycled electrode experiences slightly higher integrated-average capacitance value. Similarly, FTIR studies do not reveal any permanent changes in the shape of the spectra and

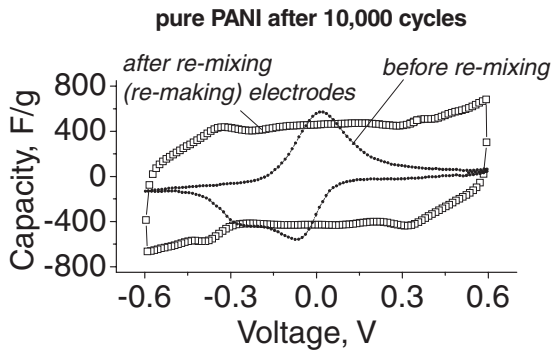

Figure 8. CV of the pure PANI electrode recorded at the sweep rate of 1 mV s^{-1} in a symmetric two-electrode configuration after 10 000 cycles before and after re-mixing/re-rolling of the electrodes.

the relative intensity of the detected peaks (Figure 9). The same results were observed for the PANI-ND composite electrodes.

3. Conclusion

In summary, we have demonstrated for the first time that low-cost detonation ND powder can greatly enhance the performance of electrochemically active polymers, such as PANI, dramatically improving their cycle stability, increasing their specific capacitance and capacitance retention at fast sweep rate. Such material improvements will ultimately lead to higher energy and power storage characteristics of PANI-based supercapacitors. ND was also found to be a good model system for systematic studies of the effects of the amount, electrical conductivity and surface structure of nanofillers on the electrochemical properties of polymer-nanopowder composites. Nanoparticles embedded in PANI were proposed to serve as a toughening agent thereby minimizing the volume changes within the PANI particles during cycling and improving electrode durability. The use of purified ND allowed us to demonstrate that the conductivity of the filler is not required for maintaining good electrical conductivity within the PANI electrode during cycling. The

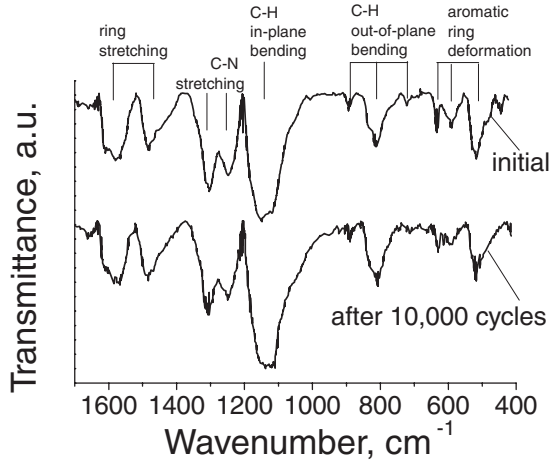

Figure 9. Fourier transform infrared spectra of the PANI electrode before and after 10 000 cycles.

existence of strong hydrogen bonding between the PANI and the filler was found to be a more important factor for the cycling stability of PANI-based composite electrodes than conductivity. Experiments with varying volume fractions of the annealed ND in PANI suggested that there is an optimum content of additives that results in the highest composite capacitance value. Adding more additives decreases capacitance and does not significantly increase electrical conductivity of the composite or improve the rate of charge-discharge. A combination of nanofiller additives imbedded into PANI during the polymerization process and conductive nanofiller additives mixed with PANI in the electrodes is needed for optimizing supercapacitor performance. To the best of our knowledge selected PANI-ND composites demonstrated one of the highest specific capacitances and the most stable performance of any PANI-based supercapacitors. An optimization of the content, distribution and the surface chemistry of ND is expected to further improve the device performance.

4. Experimental Section

ND soot and purified ND samples were obtained from NanoBlox, Inc. (PA, USA). Purification involved a combination of wet-chemical approaches to remove metal contaminants and sp^2 carbon and a dry oxidation in air to remove the remaining sp^2 carbon from the particle surface.[2] Annealing of the ND powder to transform sp^3 carbon to sp^2 carbon and produce highly conductive pure sp^2 particles[6a] was performed by heating in Ar at 1800 °C for 2h in the facilities of Solar Atmospheres Inc. (PA, USA).

Ammonium persulfate $(NH_4)_2S_2O_8$, aniline (C_6H_7N) and 1 M solution of HCl (Alfa Aesar, USA) were used for the chemical synthesis of PANI and PANI-ND (PANI-OLC) composites. The total molar ratio of C_6H_7N to $(NH_4)_2S_2O_8$ was kept at 1:1.5. After completion of the synthesis, the samples were filtered, thoroughly washed with DI water and acetone, dried at 60 °C and milled in an agate mortar into a uniform powder.

SEM studies were performed using a LEO 1530 SEM microscope (LEO, Osaka, Japan, now Nano Technology Systems Division of Carl Zeiss SMT, MA, USA). An in-lens secondary electron detector was used for the studies, most of which were performed using an accelerating voltage of 5 kV and a working distance of 3 mm. TEM observations were carried out using a JOEL 2010 microscope operated at 200 kV. To minimize the in situ transformation of diamond to graphitic carbon under the electron beam, exposure of ND samples to the electron beam was limited to 1 min. TEM samples were prepared by deposition of nanocarbon suspension onto lacey-carbon coated copper grid. FTIR spectra were collected using a Bruker Vector instrument.

The carbon-PANI electrodes for electrochemical measurements were prepared using polytetrafluoroethylene (PTFE) (60 wt% water suspension, Sigma Aldrich, USA) binder and contained 3 wt% of PTFE. After drying overnight at 60 °C under vacuum the electrodes were calendared to the thickness of ~ 400 micron using a commercial rolling mill and left to dry in the vacuum oven at 60 °C for 4–12 h prior to device assembling. The supercapacitor cells were assembled in a symmetrical two-electrode configuration. Au foil was used as a current collector. The mass loading on each electrode was 30 mg cm^{-2}. Two layers of a GORE membrane (W.L. Gore and Associates, USA), each ~25 µm in thickness and ~60% porosity, was used as a separator.

Electrochemical characterization of the materials synthesized included cyclic voltammetry (CV) in the range of –0.6 to 0.6V, electrochemical impedance spectroscopy (EIS) in the frequency range of 1 mHz to 100 kHz with a 10 mV AC amplitude and 0 V bias, and galvanostatic charge-discharge cycling in the range of 0 to 0.6 V at the current density of 6 A g^{-1}. A symmetrical cell is normally approximated as two electrode capacitors in a series. A total capacitance of the cell is thus ½ of that for each capacitor (assuming that each capacitor has the

same capacitance). The integrated-average specific capacitance of each electrode was calculated from the CV data according to

$$C_{electrode} = 2C_{cell} = \left(\frac{2}{(dU/dt)\cdot m}\right)\cdot \left\{\int_{-0.6V}^{-0.6V} I(U)dU - \int_{0.6V}^{-0.6V} I(U)dU\right\}\cdot\frac{1}{2}\cdot\frac{1}{12V}, \quad (1)$$

where dU/dt–is the scan rate, m is the mass of each electrode in a symmetric cell, and $I(U)$ is the total current. The electrode capacitance change with frequency f was calculated from the collected EIS data according to

$$C(f) = -\frac{2\cdot \mathrm{Im}(Z(f))}{2\pi f|Z(f)|^2}\cdot\left(\frac{1}{m}\right), \quad (2)$$

where Im(Z) is the imaginary component of the complex device impedance Z. The CV and EIS tests were carried out using a Zahner IM6 electrochemical workstation (Zahner-Elektrik Gmbh & CoGK, Kronach, Germany). Charge/discharge tests were performed using an Arbin SCTS supercapacitor testing system (Arbin Instruments, TN, USA). 1 M H_2SO_4 solution was used as the electrolyte for all the electrochemical measurements.

Acknowledgements

The authors thank Chuck Piccardi and Nanoblox Inc. for providing ND samples and Air Force Office of Scientific Research (grant # FA9550-09-1-0176) for partial financial support.

Received: May 6, 2010
Revised: July 13, 2010
Published online:

[1] O. Shenderova, C. Jones, V. Borjanovic, S. Hens, G. Cunningham, S. Moseenkov, V. Kuznetsov, G. McGuire, *Phys. Status Solidi A* **2008**, *205*, 2245.
[2] S. Osswald, G. Yushin, V. Mochalin, S. O. Kucheyev, Y. Gogotsi, *J. Am. Chem. Soc.* **2006**, *128*, 11635.
[3] V. L. Kuznetsov, A. L. Chuvilin, Y. V. Butenko, I. Y. Malkov, V. M. Titov, *Chem. Phys. Lett.* **1994**, *222*, 343.
[4] a) O. Shenderova, D. M. Gruen, *Ultrananocrystalline Diamond: Synthesis, Properties, and Applications*, William Andrew Publishing, Norwich New York **2006**; b) X. Q. Zhang, M. Chen, R. Lam, X. Y. Xu, E. Osawa, D. Ho, *ACS Nano* **2009**, *3*, 2609; c) M. Chen, E. D. Pierstorff, R. Lam, S. Y. Li, H. Huang, E. Osawa, D. Ho, *ACS Nano* **2009**, *3*, 2016; d) K. D. Behler, A. Stravato, V. Mochalin, G. Korneva, G. Yushin, Y. Gogotsi, *Acs Nano* **2009**, *3*, 363; e) R. Lam, M. Chen, E. Pierstorff, H. Huang, E. J. Osawa, D. Ho, *ACS Nano* **2008**, *2*, 2095; f) O. Shenderova, T. Tyler, G. Cunningham, M. Ray, J. Walsh, M. Casulli, S. Hens, G. McGuire, V. Kuznetsov, S. Lipa, *Diamond Relat. Mater.* **2007**, *16*, 1213; g) Vlasov II, O. Shenderova, S. Turner, O. I. Lebedev, A. A. Basov, I. Sildos, M. Rahn, A. A. Shiryaev, G. Van Tendeloo, *Small* **2010**, *6*, 687; h) D. A. Ho, *Acs Nano* **2009**, *3*, 3825; i) O. Faklaris, V. Joshi, T. Irinopoulou, P. Tauc, M. Sennour, H. Girard, C. Gesset, J. C. Arnault, A. Thorel, J. P. Boudou, P. A. Curmi, F. Treussart, *ACSs Nano* **2009**, *3*, 3955; j) J. Macutkevic, P. Kuzhir, D. Seliuta, G. Valusis, J. Banys, A. Paddubskaya, D. Bychanok, G. Slepyan, S. Maksimenko, V. Kuznetsov, S. Moseenkov, O. Shenderova, A. Mayer, P. Lambin, *Diamond Relat. Mater.* **2010**, *19*, 91; k) V. Borjanovic, L. Bistricic, I. Vlasov, K. Furic, I. Zamboni, M. Jaksic, O. Shenderova, *J. Vacuum Sci. Technol. B* **2009**, *27*, 2396; l) D. S. Bychanok, S. I. Moseenkov, V. L. Kuznetsov, P. P. Kuzhir, S. A. Maksimenko, K. G. Batrakov, O. V. Ruhavets, A. V. Gusinski, O. Shenderova, P. Lambin, *Journal of Nanoelectronics and Optoelectronics* **2009**, *4*, 257; m) S. Osswald, A. Gurga, F. Kellogg, K. Cho, G. Yushin, Y. Gogotsi, *Diamond Relat. Mater.* **2007**, *16*, 1967; n) G. N. Yushin, S. Osswald, V. I. Padalko, G. P. Bogatyreva, Y. Gogotsi, *Diamond Relat. Mater.* **2005**, *14*, 1721; o) E. Pecheva, L. Pramatarova, D. Fingarova, T. Hikov, I. Dineva, Z. Karagyozova, S. Stavrev, *J. Optoelectron. Adv. Mater.* **2009**, *11*, 1323; p) H. J. Huang, E. Pierstorff, E. Osawa, D. Ho, *ACS Nano* **2008**, *2*, 203; q) E. A. Ekimov, E. L. Gromnitskaya, S. Gierlotka, W. Lojkowski, B. Palosz, A. Swiderska-Sroda, J. A. Kozubowski, A. M. Naletov, *J. Mater. Sci. Lett.* **2002**, *21*, 1699; r) E. N. Loubnin, S. M. Pimenov, A. Blatter, F. Schwager, P. Y. Detkov, *New Diamond Front. Carbon Technol.* **1999**, *9*, 273; s) Y. R. Chang, H. Y. Lee, K. Chen, C. C. Chang, D. S. Tsai, C. C. Fu, T. S. Lim, Y. K. Tzeng, C. Y. Fang, C. C. Han, H. C. Chang, W. Fann, *Nat. Nanotechnol.* **2008**, *3*, 284.
[5] a) P. Simon, Y. Gogotsi, *Nat. Mater.* **2008**, *7*, 845; b) J. R. Miller, P. Simon, *Science* **2008**, *321*, 651.
[6] a) C. Portet, G. Yushin, Y. Gogotsi, *Carbon* **2007**, *45*, 2511; b) E. G. Bushueva, P. S. Galkin, A. V. Okotrub, L. G. Bulusheva, N. N. Gavrilov, V. L. Kuznetsov, S. I. Moiseekov, *Phys. Status Solidi B* **2008**, *245*, 2296.
[7] E. Frackowiak, F. Beguin, *Carbon* **2002**, *40*, 1775.
[8] a) E. Frackowiak, F. Beguin, *Carbon* **2001**, *39*, 937; b) J. Leis, M. Arulepp, A. Kuura, M. Latt, E. Lust, *Carbon* **2006**, *44*, 2122; c) D. Hulicova-Jurcakova, M. Kodama, S. Shiraishi, H. Hatori, Z. H. Zhu, G. Q. Lu, *Adv. Funct. Mater.* **2009**, *19*, 1800; d) E. Raymundo-Pinero, M. Cadek, F. Beguin, *Adv. Funct. Mater.* **2009**, *19*, 1032; e) D. Hulicova-Jurcakova, M. Seredych, G. Q. Lu, T. J. Bandosz, *Adv. Funct. Mater.* **2009**, *19*, 438; f) J. Chmiola, G. Yushin, Y. Gogotsi, C. Portet, P. Simon, *Science* **2006**, *313*, 1760; g) A. Kajdos, A. Kvit, F. Jones, J. Jagiello, G. Yushin, *J. Am. Chem. Soc.* **2010**, *132*, 3252; h) Y. Korenblit, M. Rose, E. Kockrick, L. Borchardt, A. Kvit, S. Kaskel, G. Yushin, *ACS Nano* **2010**, *4*, 1337.
[9] a) E. Frackowiak, V. Khomenko, K. Jurewicz, K. Lota, F. Beguin, *J. Power Sources* **2006**, *153*, 413; b)V. Khomenko, E. Frackowiak, F. Beguin, *Electrochim. Acta* **2005**, *50*, 2499; c) Y. K. Zhou, B. L. He, W. J. Zhou, J. Huang, X. H. Li, B. Wu, H. I. Li, *Electrochim. Acta* **2004**, *49*, 257; d) V. Gupta, N. Miura, *Electrochim. Acta* **2006**, *52*, 1721; e) L. Z. Fan, Y. S. Hu, J. Maier, P. Adelhelm, B. Smarsly, M. Antonietti, *Adv. Funct. Mater.* **2007**, *17*, 3083; f) V. Gupta, N. Miura, *Electrochem. Solid State Lett.* **2005**, *8*, A630; g) Y. G. Wang, H. Q. Li, Y. Y. Xia, *Adv. Mater.* **2006**, *18*, 2619.
[10] W. C. Chen, T. C. Wen, *J. Power Sources* **2003**, *117*, 273.
[11] a) D. W. Wang, F. Li, J. P. Zhao, W. C. Ren, Z. G. Chen, J. Tan, Z. S. Wu, I. Gentle, G. Q. Lu, H. M. Cheng, *ACS Nano* **2009**, *3*, 1745; b) L. J. Cote, R. Cruz-Silva, J. X. Huang, *J. Am. Chem. Soc.* **2009**, *131*, 11027; c) H. Bai, Y. X. Xu, L. Zhao, C. Li, G. Q. Shi, *Chem. Commun.* **2009**, 1667; d) J. Yan, T. Wei, B. Shao, Z. J. Fan, W. Z. Qian, M. L. Zhang, F. Wei, *Carbon* **2010**, *48*, 487; e) L. Zhao, Y. X. Xu, T. F. Qiu, L. J. Zhi, G. Q. Shi, *Electrochim. Acta* **2009**, *55*, 491; f) A. V. Murugan, T. Muraliganth, A. Manthiram, *Chem. Mater.* **2009**, *21*, 5004.
[12] A. Magasinski, P. Dixon, B. Hertzberg, A. Kvit, J. Ayala, G. Yushin, *Nat. Mater.* **2010**, *9*, 353.
[13] a) E. Hershkovits, A. Tannenbaum, R. Tannenbaum, *J. Phys. Chem. B* **2008**, *112*, 5317; b) E. Hershkovits, A. Tannenbaum, R. Tannenbaum, *Macromolecules* **2008**, *41*, 3190.
[14] R. De Levie, *Electrochim. Acta* **1963**, *8*, 751.
[15] P. Zoltowski, *J. Electroanal. Chem.* **1998**, *443*, 149.
[16] P. L. Taberna, P. Simon, J. F. Fauvarque, *J. Electrochem. Soc.* **2003**, *150*, A292.